Journal of Materials Chemistry A

PAPER

View Article Online
View Journal | View Issue

Cite this: J. Mater. Chem. A, 2015, 3, 17106

Metal hydroxide – a new stabilizer for the construction of sulfur/carbon composites as high-performance cathode materials for lithium–sulfur batteries

Xiao-qing Niu,[a] Xiu-li Wang,*[a] Dong-huang Wang,[a] Yi Li,[a] Yi-jun Zhang,[a] Yi-di Zhang,[a] Tao Yang,[a] Ting Yu[b] and Jiang-ping Tu[a]

Received 27th April 2015
Accepted 17th July 2015

DOI: 10.1039/c5ta03062e

www.rsc.org/MaterialsA

Rational design and fabrication of advanced sulfur cathodes is highly desirable for the development of high performance lithium–sulfur (Li–S) batteries. Herein, we report $Co(OH)_2$ as a new stabilizer for the sulfur cathode by constructing a cobalt hydroxide-covered sulfur/conductive carbon black (CCB) electrode with the help of thermal and hydrothermal treatments. In this composite, ($Co(OH)_2$@S/CCB), the sublimed sulfur is anchored in the CCB, followed by a uniform coating of $Co(OH)_2$ nanosheets. As cathode materials of lithium–sulfur batteries, the as-prepared $Co(OH)_2$@S/CCB electrode exhibits remarkable electrochemical performances with a high capacity of 1026 mA h g^{-1} at 0.1C (1C = 1675 mA g^{-1}) and 829 mA h g^{-1} at 1C. Moreover, it maintains high coulombic efficiencies above 97% after 200 cycles at 1C, much higher than those of the S/CCB counterpart electrode (85%). After 200 cycles at 1C, a high capacity retention of 71.2% is obtained, better than that of the S/CCB electrode (20.2%). The enhanced performance is mainly due to the $Co(OH)_2$ layer which helps to inhibit the shuttle diffusion of polysulfides, resulting in improved capacity retention and cycling life.

Introduction

Over the past decades, substantial effort has been made to develop green energy sources to meet the ever-increasing global energy demand and reduce environmental pollution. Among the various energy storage systems, electrochemical energy storage (EES) devices (such as batteries and supercapacitors) have been extensively studied and considered to be one of the most fascinating green energy storage systems for realizing the renewable energy future of the mankind due to their high efficiency, versatility, and flexibility.[1,2] Noticeably, lithium ion batteries (LIBs) are the most important and widely used rechargeable batteries due to their high working voltage, high capacity, low toxicity and long cycling life.[3–5] But they still fall short of meeting the demands of large-energy and high-power applications, especially for renewable energy and electric-transportation fields.[6,7] Hence, high-performance LIBs with large energy density and high power density are still highly desirable.

Lithium–sulfur (Li–S) batteries have attracted great attention in recent years, since they adopt high-capacity sulfur cathodes with a high theoretical specific capacity of 1675 mA h g^{-1} and an energy density of 2500 W h kg^{-1}, much higher than those of commercial cathode materials such as $LiCoO_2$,[8] $LiFePO_4$,[9,10] $LiMnO_2$ (ref. 11) and $LiNi_{1/3}Mn_{1/3}Co_{1/3}O_2$,[12,13] which possess energy densities of no more than 250 W h kg^{-1}. In addition, sulfur cathodes also possess advantages of low cost, natural abundance, and nontoxicity.[14,15] However, the practical application of sulfur cathodes is severely hindered by several serious problems. Firstly, the low ionic and electronic conductivities of sulfur are unfavorable for high-rate capability which requires fast ion/electron transfer. Secondly, the high solubility and "shuttle effect" of polysulfides (Li_2S_n, $4 \leq n \leq 8$) will cause loss of active materials and lower capacity.[16,17] Thirdly, the volumetric expansion during the lithiation process due to the different densities of S_8 and Li_2S will cause the cracking and fracturing of the electrode structure.[18,19] In order to overcome these problems, great efforts have been made to modify the sulfur cathode. One of the effective solutions is to construct highly porous carbon supported sulfur cathodes (sulfur/carbon composites).[20,21] Active S is stored and anchored in highly conductive and porous carbon materials (such as carbon black,[22] activated carbon,[23] porous carbon,[24–27] graphene or graphene oxide[28,29] or carbon nanotubes/nanofibers[30,31]), and enhanced electrochemical performance has been demonstrated

[a]State Key Laboratory of Silicon Materials, Key Laboratory of Advanced Materials and Applications for Batteries of Zhejiang Province, School of Materials Science and Engineering, Zhejiang University, Hangzhou 310027, China. E-mail: wangxl@zju.edu.cn

[b]Division of Physics and Applied Physics, School of Physical and Mathematical Science, Nanyang Technological University, Singapore 637371, Singapore

in these composites. For example, Ji *et al.*[26] used mesoporous CMK-3 carbon (a large pore volume of 2.1 cm^3 g^{-1} and a uniform pore size of 3.3 nm) as the sulfur host for preparation of S/CMK-3 carbon composites and higher utilization of sulfur was proven. Porous carbon materials not only provide a fast electron transfer rate, but also prohibit the dissolution of active sulfur, resulting in better cycling life and higher capacity.

Despite these advantages, the single combination between porous carbon and sulfur is still insufficient for high performances, because part of the active sulfur will escape from the outer open structure of carbon, leading to obvious capacity decay during the cycling process. It would be beneficial to form a thin sheath to the surface of the S/C composite to hinder the shuttle of sulfur and also to maintain structural stability.[32–35] Previously, Ji *et al.*[26] adopted polyethylene glycol (PEG) as a surface modifier for the S/CMK-3 composite and obtained a high initial capacity of 1320 mA h g^{-1}. Only 25% active mass was lost in the electrolyte after 30 cycles due to the trapping effect of the PEG modification. Therefore, the rational design and smart combination of sulfur, carbon materials and a protective coating layer would be an effective way to enhance the electrochemical performance of sulfur cathodes.

Different from previous modification work of sulfur cathodes, herein, we report $Co(OH)_2$ as a new coating stabilizer for the construction of high-performance sulfur/carbon composites, in which conductive carbon black (CCB) serves as the conductive matrix for the preparation of sulfur/carbon composites, and $Co(OH)_2$ nanosheets act as the layer stabilizer to restrict the diffusion of the polysulfides. The electrochemical properties of the $Co(OH)_2$@S/CCB electrode are thoroughly investigated. The as-prepared $Co(OH)_2$@S/CCB electrode exhibits better electrochemical performances than the S/CCB electrode without layer protection. Our research may provide a new way for the fabrication of stable and high-performance sulfur cathodes.

Experimental

Preparation of the $Co(OH)_2$@S/CCB composite

The synthesis process is schematically shown in Fig. 1. The commercialized conductive carbon black and sublimed sulfur were dried at 60 °C for 12 h before use. First, the S/CCB composite was prepared by grinding the conductive carbon black and sublimed sulfur in a mortar with the mass ratio of $m_s/m_c = 3/2$. After homogenous mixing, the precursors were put into a vial, which was then transferred to an autoclave with a Teflon liner and was kept at 155 °C for 24 h.

The $Co(OH)_2$@S/CCB composite was synthesized by a simple hydrothermal method. In a typical experiment, 0.05 M $Co(NO_3)_2 \cdot 6(H_2O)$ and 0.025 M $C_6H_{12}N_4$ were dissolved in deionized water, followed by magnetic stirring for 30 min, and then 0.3 g of the S/C composite were added under stirring and ultrasonication to form a stable aqueous dispersion. After that, the mixture was transferred to a 100 mL autoclave and heated at 90 °C for 2 h. After cooling to room temperature, the product was sequentially washed and filtered with deionized water several times. Then the product was dried in a vacuum oven at 60 °C overnight.

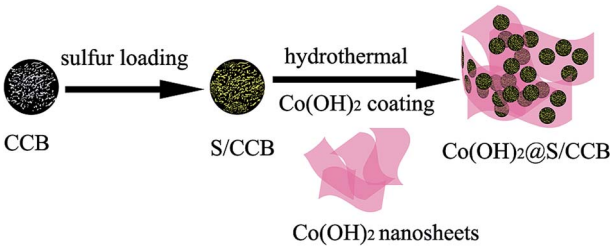

Fig. 1 Schematic illustration of the formation of the S/CCB composite and $Co(OH)_2$@S/CCB composite.

Characterization and electrochemical measurements

X-ray diffraction (XRD) patterns of the materials were characterized by using a RIGAKUD/Max-2550 in the 2-theta range of 10–70° with Cu Kα radiation. Raman spectra were scanned from 800 to 2200 cm^{-1} on an argon laser Raman spectroscope using the 514 nm laser wavelength (Labor Raman Series, HR-800). X-ray photoelectron spectroscopy (XPS) tests were carried out on an ESCALAB 250Xi system. TGA was conducted to determine the sulfur content of the materials, on a Mettler Toledo SDTQ600 instrument from room temperature to 500 °C employing a heating rate of 10 °C min^{-1} under a N_2 atmosphere. Inductively Coupled Plasma Atomic Emission Spectrometry (ICP-AES) was employed to identify the amount of $Co(OH)_2$ in the composite using an IRIS Intrepid II, Thermo Fisher Scientific. SEM studies conducted on a SU-70 field emission scanning electron-microscopy instrument and TEM performed on a JEM 2100F HRTEM were used to characterize the structures and morphologies of the as-synthesized materials.

The working electrodes were prepared from a slurry consisting of 70 wt% $Co(OH)_2$@S/CCB composites, 20 wt% conductive carbon black and 10 wt% polyvinylidene fluoride (PVDF) in *N*-methyl-2-pyrrolidone (NMP). The slurry was then coated on an aluminum foil and dried at 60 °C for 24 h in a vacuum to remove the adsorbed water from the composite. The electrolyte was 1 M bis(trifluoromethane)sulfonamide lithium salt (LiTFSI) in a mixed solvent of 1,3-dioxolane (DOL) and 1,2-dimethoxyethane (DME) with a volume ratio of 1 : 1, including 1 wt% $LiNO_3$ as an electrolyte additive, lithium metal was used as the counter and reference electrodes, and a polypropylene micro-porous film (Cellgard 2300) was used as the separator. 2025-type coin cells were assembled in an argon-filled glove box. Cyclic voltammograms (CVs) were obtained with a CHI 660D electrochemical workstation in the potential range of 1.5–3.0 V (Li/Li^+) at a scan rate of 0.1 mV s^{-1}. Electrochemical impedance spectroscopy (EIS) measurements were conducted over a frequency range of 100 kHz to 10 mHz by applying an AC signal of 5 mV. The galvanostatic discharge/charge was performed on a LAND battery program-control test system (Wuhan, China) between 1.6 and 2.7 V at room temperature. The cathodes were activated at C/20 (1C = 1675 mA g^{-1}) in the first two cycles.

Results and discussion

The XRD patterns of the pristine CCB, elemental sulfur, synthesized $Co(OH)_2$, S/CCB composite and $Co(OH)_2$@S/CCB composite are shown in Fig. 2a. For the pristine CCB, the strong peak at 25° suggests that the CCB is partially graphitized and the weak peak at 42° indicates the quasi-amorphous frameworks.[36] Sulfur showed typical XRD diffraction peaks at 23° and 28°, which correspond to an *Fddd* orthorhombic structure.[37,38] All the diffraction peaks in the XRD pattern of the synthesized $Co(OH)_2$ can be indexed to a hexagonal $Co(OH)_2$ phase, in good agreement with that of the standard values (JCPDF 74-1057). For the S/CCB composite and $Co(OH)_2$@S/CCB composite, the XRD patterns show the characteristic peaks of S, with the peak positions remaining the same as in the case of elemental sulfur, suggesting that the crystal structure of S is unchanged and no new phase is formed during the composite preparation. Raman spectroscopy is a powerful technique for characterizing carbonaceous materials, the Raman spectrum of the $Co(OH)_2$@S/CCB composite is shown in Fig. 2b. Obviously, there are two broad peaks present at ~1346 and ~1585 cm^{-1}, which correspond to the D and G bands of graphite,[39,40] respectively, confirming the existence of the conductive carbon black (CCB). To verify the existence of $Co(OH)_2$ in the $Co(OH)_2$@S/CCB composite, The XPS test was applied. All peaks are referenced to the C 1s line at a binding energy of 284.8 eV and the core peaks are analyzed using a nonlinear Shirley-type background, the related peak positions and areas are optimized by a weighted least squares fitting method. Fig. 2c and d show the Co 2p and O 1s XPS spectra of the $Co(OH)_2$@S/CCB composite, respectively. The Co 2p spectrum shows spin–orbit splitting into $2p_{1/2}$ and $2p_{3/2}$ components, and both components qualitatively contain the same chemical information.[41] Therefore, in our study, only Co $2p_{3/2}$ bands are curve-fitted. In the Co $2p_{3/2}$ spectrum (Fig. 2c), three main peaks at ~780.7, ~782.6 and ~786.3 eV are observed, which are fitted for $Co(OH)_2$. For the O 1s (Fig. 2d), an intense band at 531.1 eV is obviously observed, which is considered to be the O from the hydroxide ions.[42–44] Low peaks in the spectrum are ascribed to hydroxyl and carbonate ion contamination on the surface of the composite.[45] All of the above results imply that $Co(OH)_2$ is formed in the $Co(OH)_2$@S/CCB composite.

TGA was applied to determine the sulfur content in the composites. As shown in Fig. 3, sulfur completely evaporates at 330 °C, at the same time, carbon remains approximately unchanged. The dehydration of $Co(OH)_2$ is a multi-step process. In the first step, a mass loss of 15.09% occurs in the range of 25–150 °C, attributed to the adsorbed water and intercalated water species loss. 18.4% mass loss is observed in the following step due to the decomposition of $Co(OH)_2$ to CoO beginning at 200 °C. Most of the weight loss ends at 300 °C, but a continuous tiny loss is seen up to 500 °C.[46–48] The TG curve of the $Co(OH)_2$@S/CCB composite is similar to that of the S/CCB composite with an approximate weight loss due to the low content of the $Co(OH)_2$ in the composite. And because of the overlapped weightlessness temperature range of $Co(OH)_2$ and sulfur, it is not possible to determine the sulfur content in the $Co(OH)_2$@S/CCB composite only by TGA. Here, ICP was used to measure the Co content in the $Co(OH)_2$@S/CCB composite. ICP analysis shows a mass percent of 1.18% of the $Co(OH)_2$ in the composite. Along with the fixed ratio of S and CCB (3/2), the final sulfur content in the composite is 59.29 wt%.

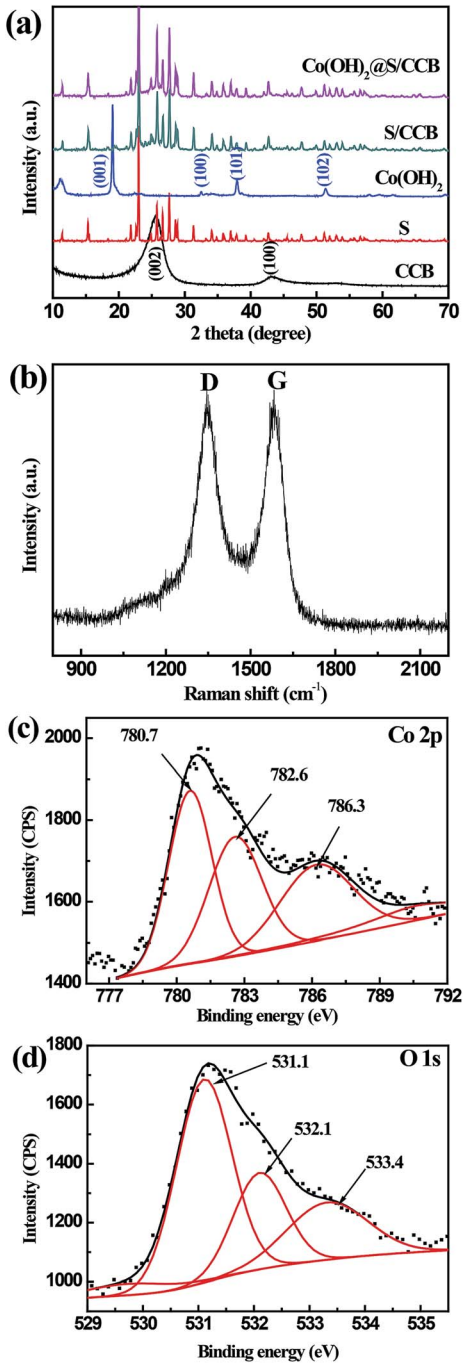

Fig. 2 (a) XRD patterns of the pristine CCB, element sulfur, synthesized $Co(OH)_2$, S/CCB composite and $Co(OH)_2$@S/CCB composite; (b) Raman spectrum of the $Co(OH)_2$@S/CCB composite (800–2200 cm^{-1}). XPS high-resolution spectra of (c) Co 2p, (d) O 1s obtained from the $Co(OH)_2$@S/CCB composite.

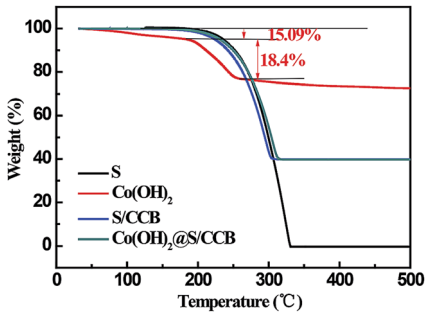

Fig. 3 TG curves of the S, $Co(OH)_2$, S/CCB composite and $Co(OH)_2$@S/CCB composite.

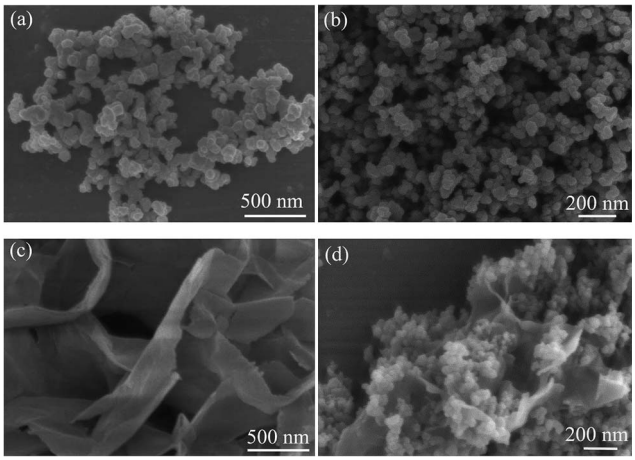

Fig. 4 SEM images of the (a) CCB; (b) S/CCB composite; (c) $Co(OH)_2$ nanosheets; (d) $Co(OH)_2$@S/CCB composite.

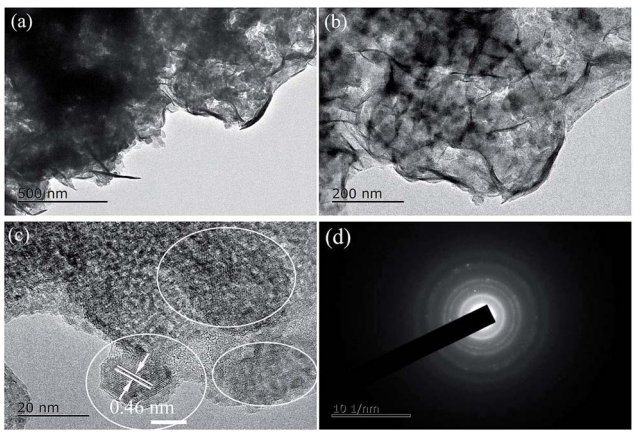

Fig. 5 (a and b) TEM images; (c) the high-resolution TEM (HRTEM) image; (d) the corresponding SAED pattern of the $Co(OH)_2$@S/CCB composite.

Fig. 4 presents the SEM images of the CCB, S/CCB composite, $Co(OH)_2$ nanosheets and $Co(OH)_2$@S/CCB composite. The CCB looks like a particle aggregation of many small and uniform spheres with an average size of less than 100 nm (Fig. 4a). After heat-treatment with sulfur, the spherical morphology of the CCB is still retained, but the aggregations become denser (Fig. 4b). It has been put forward that melted sulfur heat-treated at 155 °C with a low viscosity can diffuse into the pores of the CCB by a capillary force.[49] As seen in Fig. 4c, the synthesized $Co(OH)_2$ exhibits a flower-like morphology assembled by three dimensionally (3D) connected thin nanosheets. The S/CCB nanospheres are embedded in the 3D $Co(OH)_2$ nanosheets in the $Co(OH)_2$@S/CCB composite (Fig. 4d). The 3D structure provides intersected blocks for polysulfides during the cycling process, making them constantly change the diffusion direction, thus mitigating the diffusion of the polysulfides into the electrolyte. TEM was further used to examine the $Co(OH)_2$@S/CCB composite. The S/CCB nanospheres aggregate together and are wrapped by ultrathin $Co(OH)_2$ nanosheets (Fig. 5a and b). The high-resolution TEM (HRTEM) image in Fig. 5c exhibits a 0.46 nm lattice spacing corresponding to the (001) planes of $Co(OH)_2$ (JCPDF 74-1057), supported by the XRD data. The selected area electron diffraction pattern of the $Co(OH)_2$@S/CCB composite reveals the coexistence of the amorphous carbon and crystalline $Co(OH)_2$ phase (Fig. 5d). However, diffraction rings of sulfur are not observed. This is possibly because sulfur is sublimated under the high energy electron beam.[50] It is believed that this structure can effectively protect S and the formed polysulfides from diffusing into the electrolyte.

Cyclic voltammograms and charge/discharge profiles at 0.1C of the S/CCB electrode and $Co(OH)_2$@S/CCB electrode are shown in Fig. 6. The plots in Fig. 6a show typical electrochemical reaction characteristics of the elemental sulfur, the two main reduction peaks at potentials of 2.3 V and 2.0 V correspond to the formation of long-chain Li_2S_n ($4 \leq n < 8$) and short-chain Li_2S_2/Li_2S, respectively. The oxidation peak at around 2.4 V is attributed to its reverse process.[51,52] Compared with the S/CCB electrode, the $Co(OH)_2$@S/CCB electrode shows a little lower but more stable oxidation peak, suggesting that the $Co(OH)_2$ nanosheets can effectively prevent S and polysulfides from diffusing into the electrolyte, hence keeping the cathodes stable. Interestingly, there is an extra shoulder peak at 2.37 V in the S/CCB electrode during the oxidation process, indicating that two oxidative peaks exist and overlap with each other (Fig. 6b). Similar behaviors have also been observed in previous studies.[53–56]

The charge/discharge profiles of the S/CCB electrode and $Co(OH)_2$@S/CCB electrode at 0.1C are shown in Fig. 6c. Consistent with the results from CV, the typical two-plateau behavior of the sulfur electrode is observed. For the charge/discharge curves of the S/CCB electrode, although a little higher initial capacity of 1052 mA h g^{-1} is obtained, the discharge capacity decreases very quickly to 841 mA h g^{-1} after ten cycles, which demonstrates severe loss of active materials.[51] In contrast, there is an activation process in the initial ten cycles for the $Co(OH)_2$@S/CCB electrode. A similar phenomenon has been observed when using reduced graphene oxide (rGO) as a barrier.[57] We may suggest this activation process as follows. The polysulfides generated in the previous cycles are inhibited and attach onto the $Co(OH)_2$ nanosheets, then the active materials redistribute to a more homogenous state during cycling and the

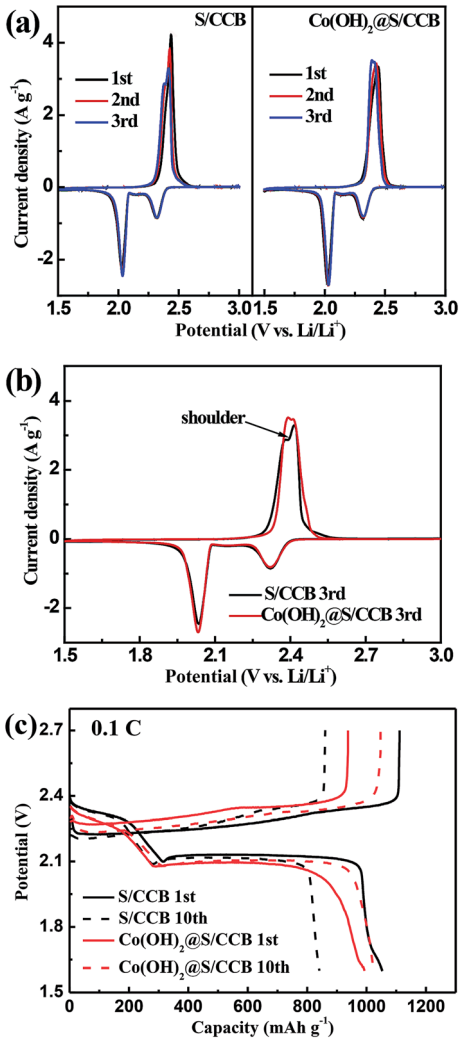

Fig. 6 (a) CV curves; (b) the third cycle of the CV curves; (c) discharge/charge voltages at 0.1C of the S/CCB electrode and $Co(OH)_2$@S/CCB electrode.

utilization of sulfur increases. A maximum discharge capacity of 1026 mA h g^{-1} is obtained after activation.

The cycling performances, coulombic efficiencies and rate capacities of the S/CCB electrode and $Co(OH)_2$@S/CCB electrode are investigated and shown in Fig. 7. A favorable cycling performance is a manifestation of effective retardation of the polysulfide shuttle reaction. An initial capacity of the S/CCB electrode, ~1053 mA h g^{-1} at 0.1C is obtained, which is a little higher than that of the $Co(OH)_2$@S/CCB electrode (~993 mA h g^{-1}). Meanwhile, more degradation of capacity occurs in the S/CCB electrode (retaining ~645 mA h g^{-1} at 0.1C after 100 cycles, ~193 mA h g^{-1} at 1C after 200 cycles) in contrast with the $Co(OH)_2$@S/CCB electrode (retaining ~779 mA h g^{-1} at 0.1C after 100 cycles, ~576 mA h g^{-1} at 1C after 200 cycles) (Fig. 7a and b). The coulombic efficiency of the $Co(OH)_2$@S/CCB electrode remains at above 97% after 200 cycles at 1C, which is higher than that of the S/CCB electrode (85%) (Fig. 7b), indicating that the polysulfide is effectively entrapped owing to the $Co(OH)_2$ coating on the surface of the S/CCB composite. Furthermore, although $Co(OH)_2$ bears unfavorable conductivity, a better rate performance is notably observed for the $Co(OH)_2$@S/CCB electrode, showing the importance of the better trap of sulfur with the coating of the $Co(OH)_2$ layer. The discharge capacities are stabilized around 1000, 860, 780 and 730 mA h g^{-1} when cycling at 0.1, 0.2, 0.5 and 1C, respectively. When the current rate is switched abruptly to 0.1C, the capacity is recovered to 880 mA h g^{-1} (Fig. 7c), which is

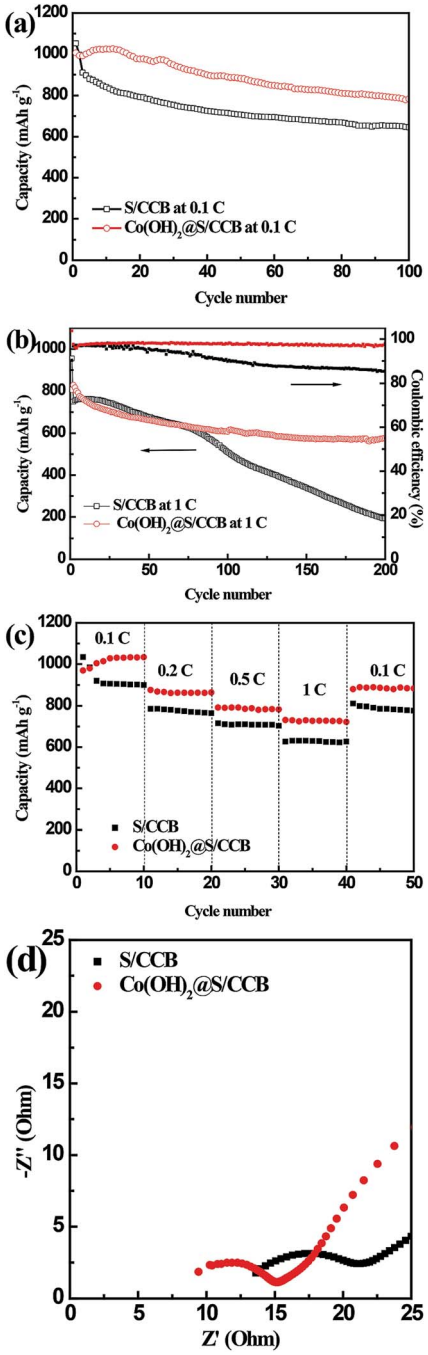

Fig. 7 (a) Cycle stability at 0.1C; (b) cycling performances and coulombic efficiencies at 1C; (c) rate capabilities; (d) Nyquist plots of the S/CCB electrode and $Co(OH)_2$@S/CCB electrode after ten cycles at 1C, frequency range: 100 kHz to 10 mHz.

equivalent to the value at the 40th cycle shown in Fig. 7a, suggesting the stability of the $Co(OH)_2$@S/CCB electrode.

EIS spectra of the S/CCB electrode and $Co(OH)_2$@S/CCB electrode after 10 cycles at 1C are measured and shown in Fig. 7d. Both of the impedance plots display a semicircle in the high–medium frequency region, relating to the charge transfer resistance at the interface, and an inclined line in the low frequency region, which corresponds to the semi-infinite Warburg diffusion process.[39,58] The $Co(OH)_2$@S/CCB electrode shows a slightly smaller semicircle diameter than the S/CCB electrode, indicating good charge transport and electrolyte infiltration as well as effective reutilization/entrapment of dissolved sulfur and polysulfides, thereby mitigating the formation of the passivation layer (Li_2S_2/Li_2S) on the lithium anodes.[54] Furthermore, the electrolyte resistance (intersection between the initial part of the high frequency semicircle and the real axis), which is related to the viscosity of the polysulfides in the electrolyte,[40,53,59] in the $Co(OH)_2$@S/CCB electrode is smaller compared to that in the S/CCB electrode, suggesting that less long-chain polysulfides diffuse into the electrolyte. The improved polysulfide-entrapment capacity verifies that this $Co(OH)_2$@S/CCB electrode configuration is promising to solve the persistent problem of capacity fading.

Conclusions

In summary, we have demonstrated a metal hydroxide ($Co(OH)_2$) layer coating for the construction of advanced multi-component sulfur cathodes and their enhanced electrochemical performances. The $Co(OH)_2$ nanosheet is proven to be a promising protective layer material for high-performance sulfur cathodes because of the effective trapping effect for polysulfides. Due to the unique composite, the $Co(OH)_2$@S/CCB electrode shows excellent electrochemical performances with higher capacity, and better cycling performance as compared to the S/CCB electrode. This metal hydroxide layer modification can be used as an effective approach for the fabrication of high-performance sulfur cathodes.

Acknowledgements

This work is supported by the National Natural Science Foundation of China (no. 51271167) and Program for Innovative Research Team in University of Ministry of Education of China (no. IRT13037).

References

1 S. Brown, D. Pyke and P. Steenhof, *Energy Policy*, 2010, **38**, 3797–3806.
2 R. Marom, S. F. Amalraj, N. Leifer, D. Jacob and D. Aurbach, *J. Mater. Chem.*, 2011, **21**, 9938–9954.
3 J.-M. Tarascon and M. Armand, *Nature*, 2001, **414**, 359–367.
4 M. S. Whittingham, *Chem. Rev.*, 2004, **104**, 4271–4302.
5 N. S. Choi, Z. H. Chen, S. A. Freunberger, X. L. Ji, Y. K. Sun, K. Amine, G. Yushin, L. F. Nazar, J. Cho and P. G. Bruce, *Angew. Chem., Int. Ed.*, 2012, **51**, 9994–10024.
6 D. Bresser, S. Passerini and B. Scrosati, *Chem. Commun.*, 2013, **49**, 10545–10562.
7 A. Manthiram, *J. Phys. Chem. Lett.*, 2011, **2**, 176–184.
8 Q. Cao, H. P. Zhang, G. J. Wang, Q. Xia, Y. P. Wu and H. Q. Wu, *Electrochem. Commun.*, 2007, **9**, 1228–1232.
9 W. L. Liu, J. P. Tu, Y. Q. Qiao, J. P. Zhou, S. J. Shi, X. L. Wang and C. D. Gu, *J. Power Sources*, 2011, **196**, 7728–7735.
10 A. Fedorková, R. Oriňáková, A. Oriňák, H.-D. Wiemhöfer, D. Kaniansky and M. Winter, *J. Solid State Electrochem.*, 2010, **14**, 2173–2178.
11 I. Koetschau, M. Richard, J. Dahn, J. Soupart and J. Rousche, *J. Electrochem. Soc.*, 1995, **142**, 2906–2910.
12 T. Ohzuku and Y. Makimura, *Chem. Lett.*, 2001, **30**, 642–643.
13 S. J. Shi, J. P. Tu, Y. J. Mai, Y. Q. Zhang, C. D. Gu and X. L. Wang, *Electrochim. Acta*, 2012, **63**, 112–117.
14 M. He, L.-X. Yuan, W.-X. Zhang, X.-L. Hu and Y.-H. Huang, *J. Phys. Chem. C*, 2011, **115**, 15703–15709.
15 P. Guo, H. H. Song and X. H. Chen, *Electrochem. Commun.*, 2009, **11**, 1320–1324.
16 D. Wang, Y. C. Yu, W. D. Zhou, H. Chen, F. J. DiSalvo, D. A. Muller and H. D. Abruña, *Phys. Chem. Chem. Phys.*, 2013, **15**, 9051–9057.
17 Q. Zhao, X. F. Hu, K. Zhang, N. Zhang, Y. X. Hu and J. Chen, *Nano Lett.*, 2015, **15**, 721–726.
18 Y. Zhao, W. L. Wu, J. X. Li, Z. C. Xu and L. H. Guan, *Adv. Mater.*, 2014, **26**, 5113–5118.
19 X. Zhao, J.-K. Kim, H.-J. Ahn, K.-K. Cho and J.-H. Ahn, *Electrochim. Acta*, 2013, **109**, 145–152.
20 M. M. Rao, X. Y. Song and E. J. Cairns, *J. Power Sources*, 2012, **205**, 474–478.
21 C. F. Zhang, H. B. Wu, C. Z. Yuan, Z. P. Guo and X. W. D. Lou, *Angew. Chem.*, 2012, **124**, 9730–9733.
22 J. Shim, K. A. Striebel and E. J. Cairns, *J. Electrochem. Soc.*, 2002, **149**, A1321.
23 J. L. Wang, L. Liu, Z. J. Ling, J. Yang, C. R. Wan and C. Y. Jiang, *Electrochim. Acta*, 2003, **48**, 1861–1867.
24 S. C. Wei, H. Zhang, Y. Q. Huang, W. K. Wang, Y. Z. Xia and Z. B. Yu, *Energy Environ. Sci.*, 2011, **4**, 736–740.
25 X. L. Li, Y. L. Cao, W. Qi, L. V. Saraf, J. Xiao, Z. M. Nie, J. Mietek, J.-G. Zhang, B. Schwenzer and J. Liu, *J. Mater. Chem.*, 2011, **21**, 16603–16610.
26 X. L. Ji, K. T. Lee and L. F. Nazar, *Nat. Mater.*, 2009, **8**, 500–506.
27 G. He, X. L. Ji and L. Nazar, *Energy Environ. Sci.*, 2011, **4**, 2878–2883.
28 C. X. Zu and A. Manthiram, *Adv. Energy Mater.*, 2013, **3**, 1008–1012.
29 M. K. Song, Y. G. Zhang and E. J. Cairns, *Nano Lett.*, 2013, **13**, 5891–5899.
30 G. Y. Zheng, Y. Yang, J. J. Cha, S. S. Hong and Y. Cui, *Nano Lett.*, 2011, **11**, 4462–4467.
31 W. Ahn, K.-B. Kim, K.-N. Jung, K.-H. Shin and C.-S. Jin, *J. Power Sources*, 2012, **202**, 394–399.
32 F. Wu, J. Z. Chen, R. J. Chen, S. X. Wu, L. Li, S. Chen and T. Zhao, *J. Phys. Chem. C*, 2011, **115**, 6057–6063.
33 G. C. Li, G. R. Li, S. H. Ye and X. P. Gao, *Adv. Energy Mater.*, 2012, **2**, 1238–1245.

34 X. Y. Zhao, J. P. Tu, Y. Lu, J. B. Cai, Y. J. Zhang, X. L. Wang and C. D. Gu, *Electrochim. Acta*, 2013, **113**, 256–262.
35 S. T. Lu, Y. W. Cheng, X. H. Wu and J. Liu, *Nano Lett.*, 2013, **13**, 2485–2489.
36 S. Evers and L. F. Nazar, *Chem. Commun.*, 2012, **48**, 1233–1235.
37 C. Y. Zhao, L. J. Liu, H. L. Zhao, A. Krall, Z. H. Wen, J. H. Chen, P. Hurley, J. W. Jiang and Y. Li, *Nanoscale*, 2014, **6**, 882–888.
38 Y. Z. Fu and A. Manthiram, *RSC Adv.*, 2012, **2**, 5927–5929.
39 S. Y. Zheng, Y. Wen, Y. J. Zhu, Z. Han, J. Wang, J. H. Yang and C. S. Wang, *Adv. Energy Mater.*, 2014, **4**, 482–491.
40 Y.-X. Wang, L. Huang, L.-C. Sun, S.-Y. Xie, G.-L. Xu, S.-R. Chen, Y.-F. Xu, J.-T. Li, S.-L. Chou and S.-X. Dou, *J. Mater. Chem.*, 2012, **22**, 4744–4750.
41 K. Artyushkova, S. Levendosky, P. Atanassov and J. Fulghum, *Top. Catal.*, 2007, **46**, 263–275.
42 J. Haber, J. Stoch and L. Ungier, *J. Electron Spectrosc. Relat. Phenom.*, 1976, **9**, 459–467.
43 N. McIntyre and M. Cook, *Anal. Chem.*, 1975, **47**, 2208–2213.
44 J. Yang, H. W. Liu, W. N. Martens and R. L. Frost, *J. Phys. Chem. C*, 2010, **114**, 111–119.
45 J. Stoch and J. Gablankowska Kukucz, *Surf. Interface Anal.*, 1991, **17**, 165–167.
46 K. Zhang, Q. Zhao, Z. L. Tao and J. Chen, *Nano Res.*, 2013, **6**, 38–46.
47 M. Rajamathi, P. V. Kamath and R. Seshadri, *Mater. Res. Bull.*, 2000, **35**, 271–278.
48 J. T. Sampanthar and H. C. Zeng, *J. Am. Chem. Soc.*, 2002, **124**, 6668–6675.
49 Y. L. Cao, X. L. Li, I. A. Aksay, J. Lemmon, Z. M. Nie, Z. G. Yang and J. Liu, *Phys. Chem. Chem. Phys.*, 2011, **13**, 7660–7665.
50 Y. Liu, J. X. Guo, J. Zhang, Q. M. Su and G. H. Du, *Appl. Surf. Sci.*, 2015, **324**, 399–404.
51 J. Schuster, G. He, B. Mandlmeier, T. Yim, K. T. Lee, T. Bein and L. F. Nazar, *Angew. Chem., Int. Ed.*, 2012, **51**, 3591–3595.
52 L. F. Xiao, Y. L. Cao, J. X. Xiao, B. Schwenzer, M. H. Engelhard, L. V. Saraf, Z. Nie, G. J. Exarhos and J. Liu, *Adv. Mater.*, 2012, **24**, 1176–1181.
53 C. X. Zu, Y. Z. Fu and A. Manthiram, *J. Mater. Chem. A*, 2013, **1**, 10362–10367.
54 H. F. Li, X. W. Yang, X. M. Wang, M. N. Liu, F. M. Ye, J. Wang, Y. C. Qiu, W. F. Li and Y. G. Zhang, *Nano Energy*, 2015, **12**, 468–475.
55 M. M. Sun, S. C. Zhang, T. Jiang, L. Zhang and J. H. Yu, *Electrochem. Commun.*, 2008, **10**, 1819–1822.
56 Y. Yang, G. H. Yu, J. J. Cha, H. Wu, M. Vosgueritchian, Y. Yao, Z. N. Bao and Y. Cui, *ACS Nano*, 2011, **5**, 9187–9193.
57 X. F. Wang, Z. X. Wang and L. Q. Chen, *J. Power Sources*, 2013, **242**, 65–69.
58 G. M. Zhou, S. F. Pei, L. Li, D. W. Wang, S. G. Wang, K. Huang, L. C. Yin, F. Li and H. M. Cheng, *Adv. Mater.*, 2014, **26**, 625–631.
59 L. X. Yuan, X. P. Qiu, L. Q. Chen and W. T. Zhu, *J. Power Sources*, 2009, **189**, 127–132.